nature climate change

ARTICLES

https://doi.org/10.1038/s41558-022-01388-4

Check for updates

OPEN

Declining tropical cyclone frequency under global warming

Savin S. Chand[1]✉, Kevin J. E. Walsh[2], Suzana J. Camargo[3], James P. Kossin[4,5], Kevin J. Tory[6], Michael F. Wehner[7], Johnny C. L. Chan[8], Philip J. Klotzbach[9], Andrew J. Dowdy[6], Samuel S. Bell[6], Hamish A. Ramsay[10] and Hiroyuki Murakami[11]

Assessing the role of anthropogenic warming from temporally inhomogeneous historical data in the presence of large natural variability is difficult and has caused conflicting conclusions on detection and attribution of tropical cyclone (TC) trends. Here, using a reconstructed long-term proxy of annual TC numbers together with high-resolution climate model experiments, we show robust declining trends in the annual number of TCs at global and regional scales during the twentieth century. The Twentieth Century Reanalysis (20CR) dataset is used for reconstruction because, compared with other reanalyses, it assimilates only sea-level pressure fields rather than utilize all available observations in the troposphere, making it less sensitive to temporal inhomogeneities in the observations. It can also capture TC signatures from the pre-satellite era reasonably well. The declining trends found are consistent with the twentieth century weakening of the Hadley and Walker circulations, which make conditions for TC formation less favourable.

Human activities are estimated to have caused ~1.0 °C of global warming above pre-industrial levels, with most of the warming occurring since the mid-twentieth century[1]. This warming may have already impacted the number of tropical cyclone (TC) occurrences at global and regional scales, but so far changes are unclear—and often controversial—due to several confounding factors, including data quality issues that create major challenges for detection and attribution of TC trends[2]. Before the commencement of geostationary weather satellite monitoring in the 1970s, historical global 'best track' records of TCs were more prone to discontinuities and sampling issues and are therefore considered problematic for climate change trend analysis[2,3]. TC observations have improved substantially since the 1970s, but this relatively short period of high-quality data does not provide consensus on the detection of trends or on the attribution of trends to anthropogenic influences. On the basis of the few decades of reliable historical data, there is no clear evidence of an observed trend in global TC numbers. Trends in regional TC numbers based on observations can be obscured by natural climate variability, including at decadal to multi-decadal time scales, leading to conflicting conclusions on detection and attribution of TC frequency trends[2–7].

Several hypotheses tested using climate model experiments point to a plausible link between anthropogenic-induced greenhouse warming and changes in TC numbers at global and regional scales[8–14]. To summarize these studies, we note that TCs can form only when an initial circulation is protected from environmental wind shear and dry air intrusions[15], within which prolonged deep convection can moisten the protected region sufficiently to allow a precursor to develop into a TC[16]. Even in the current climate, much of the tropics are typically hostile to TC formation with the middle troposphere being too dry and wind shear often too strong[17]. In a warming climate, changes in deep convection, wind shear and middle tropospheric humidity are likely to contribute to an even more hostile TC formation environment globally[8–11]. At a regional scale, non-uniform sea surface temperature (SST) increase (that is, warming relative to the mean tropical SST) can cause shifts in the areas of active convection with associated changes in wind shear and middle-troposphere dryness, leading to shifts in TC formation locations[10,18,19]. But those areas of active convection caused by non-uniform SST increase are also likely to be influenced by other factors such as internal climate variability and localized aerosol effects, making it difficult to detect any long-term changes in regional TC numbers.

Given the unprecedented level of warming since the mid-twentieth century in the context of at least the past 2,000 years[1,20] and its associated impact on the major atmospheric circulations in the tropics[21–24], one would expect such changes to manifest in the total number of TCs observed globally. While most climate model experiments project a likely decline in global TC numbers due to greenhouse warming[12], studies that have attempted to assess these changes empirically are often constrained by the lack of observational data covering the pre-industrial period[2]. Palaeoclimate reconstructions do provide some indications of changes in TC activity over the period but only for localized regions, limiting the ability of this approach to realistically capture basin-wide and global-scale trends and variability[25].

Here we use the Twentieth Century Reanalysis (20CR) dataset[26] to derive a long-term historical proxy record of global TCs extending back to the mid-nineteenth century, allowing objective assessments of changes in global- and regional-scale TC numbers since 1850

[1]Institute of Innovation, Science and Sustainability, Federation University, Ballarat, Victoria, Australia. [2]University of Melbourne, Parkville, Victoria, Australia. [3]Lamont-Doherty Earth Observatory, Columbia University, Palisades, NY, USA. [4]NOAA/National Centers for Environmental Information/Climate Science and Services Division, Madison, WI, USA. [5]The Climate Service, Madison, WI, USA. [6]Research and Development Branch, Bureau of Meteorology, Melbourne, Victoria, Australia. [7]Lawrence Berkeley National Laboratory, Berkeley, CA, USA. [8]Guy Carpenter Asia-Pacific Climate Impact Centre, City University of Hong Kong, Kowloon, China. [9] Department of Atmospheric Science, Colorado State University, Fort Collins, CO, USA. [10]CSIRO, Oceans and Atmosphere, Aspendale, Victoria, Australia. [11]National Oceanic and Atmospheric Administration/Geophysical Fluid Dynamics Laboratory, Princeton, NJ, USA. ✉e-mail: s.chand@federation.edu.au

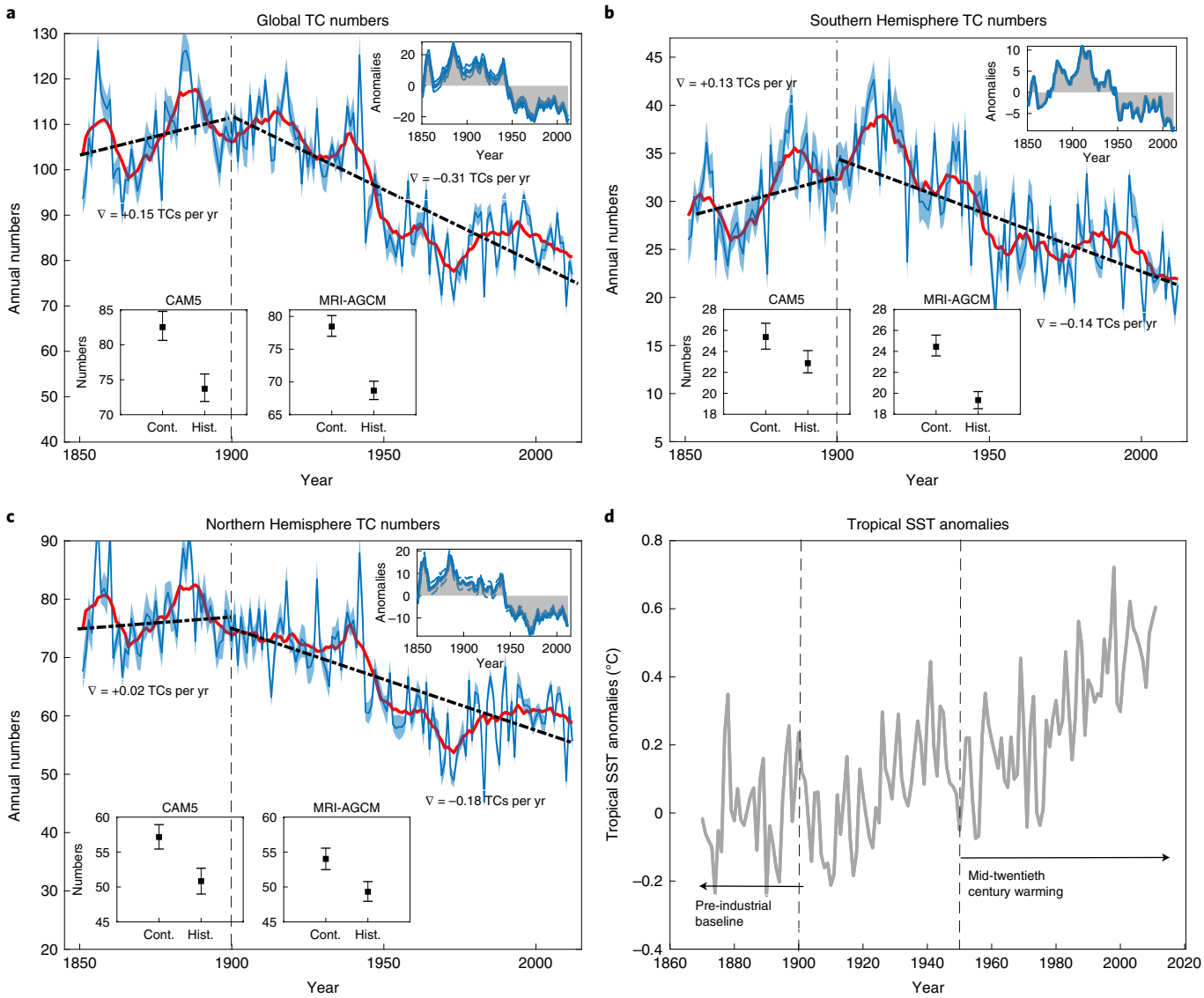

Fig. 1 | Anthropogenic greenhouse warming-induced changes in global and hemispheric annual TC numbers as inferred from the 20CR dataset and changes in the mean annual TC numbers between the pre-industrial control and historical periods as derived from climate model experiments. **a**–**c**, Time series of ensemble-mean global (**a**), Southern Hemisphere (**b**) and Northern Hemisphere (**c**) TC numbers for each year (blue solid line) and the ensemble spread at the 95% confidence interval (blue shading), long-term trends in the ensemble-mean annual TC numbers for the pre-industrial and the twentieth century periods (black dashed line and the associated gradients ∇) and the five-year running mean (red line). The inset on the top right of each panel shows the anomalies of annual TC numbers (with respect to the entire period), and the two insets on the bottom left of each panel are the results from the CAM5 and MRI-AGCM model experiments showing the mean changes in annual TC numbers (with 95% confidence intervals) between the pre-industrial control ('Cont.') and historical ('Hist.') simulations; the pre-industrial control has natural forcings only, while the historical has both natural forcing and anthropogenic components. **d**, Time series of the summertime tropical SST anomalies showing the level of warming with respect to the pre-industrial baseline and the period of warming since the mid-twentieth century. The vertical dashed line in panels a,b,c denotes a baseline approximation of the pre-industrial period ending at 1900.

(Methods). Note here that the period 1850–1900 is used as a baseline approximation of pre-industrial conditions, consistent with the definition of the Intergovernmental Panel on Climate Change (IPCC)[1]. The 20CR reanalysis assimilates only surface pressure-based observations as opposed to most other reanalyses that utilize observations at many vertical levels throughout the troposphere and stratosphere. This methodology of using all available observations has resulted in substantial inhomogeneities given the time-changing observational network[26]. Earlier studies have shown that the 20CR is an effective tool for examining TC records in an historical context[27,28]. Here we apply an innovative direct TC detection and tracking scheme that utilizes only tropospheric variables—inspired by the 'marsupial-pouch' concept of TC formation[15] termed the Okubo–Weiss–Zeta (OWZ) scheme[29,30]—to create a long-term proxy record of TCs from the 20CR for the period 1850–2012. These 20CR-derived TCs are extensively validated with the available best track records for all TC basins (Methods section on 'Statistical assessment of annual TC numbers').

In addition to the 20CR dataset, climate model experiments from two recent projects—the 'Database for Policy Decision-Making for Future Climate Change' (d4PDF)[31] and the 'International CLIVAR Climate of the Twentieth Century Plus Detection and Attribution project' (C20C+D&A)[32]—are used to explore the role of anthropogenic warming on the observed changes in global- and

Table 1 | Changes in mean annual TC numbers between the two climate periods: pre-industrial and historical

	20CR	CAM5	MRI-AGCM
Global	−13%	−11% [−15 −6]	−13% [−19 −8]
Southern Hemisphere	−7%	−10% [−18 −5]	− 20% [−26 −14]
Northern Hemisphere	−16%	−11% [−17 −4]	−9% [−16 −3]
South Pacific	−19%	−17% [−46 +1]	−34% [−45 −19]
Australian region	−11%	−14% [−28 −1]	−21% [−28 −10]
South Indian	+5%	−3% [−19 +15]	−11% [−25 +5]
North Indian	−20%	−3% [−23 +21]	+2% [−3 +26]
Western North Pacific	−9%	−8% [−18 +1]	−14% [−21 −5]
Eastern North Pacific	−18%	−8% [−18 +2]	−13% [−23 0]
North Atlantic	−42% [−28%]	−22% [−34 −12]	+10% [−8 +30]

The 95% credible intervals for the model simulations are shown in brackets. For the North Atlantic basin, the change in the 20CR-derived mean annual number after the bias correction is shown in brackets (that is, −28%).

Table 2 | As in Table 1 but for changes in mean annual TC numbers between the periods 1901–1950 and 1951–2010 for the 20CR and CERA-20C datasets

	20CR	CERA-20C
Global	−20%	−9% [−13 −1]
Southern Hemisphere	−26%	−14% [−21 −4]
Northern Hemisphere	−18%	−5% [−12 +3]
South Pacific	−40%	−17% [−42 +21]
Australian region	−32%	−24% [−30 −11]
South Indian	−15%	−1% [−18 +16]
North Indian	−27%	−15% [−30 +2]
Western North Pacific	−15%	−8% [−18 +2]
Eastern North Pacific	−28%	−16% [−29 +1]
North Atlantic*	+1%	+80% [+25 +166]

Asterisk associated with the North Atlantic indicates that CERA-20C, like many other coarse-resolution coupled climate models[43], have limitations in simulating realistic TC numbers for the basin (Supplementary Fig. 5d). Consequently, care must be exercised when interpreting the magnitude of the change computed from CERA-20C between the periods 1901–1950 and 1951–2010 for the North Atlantic basin.

regional-scale TC numbers derived from the 20CR. The two models are the Atmospheric General Circulation Model of the Meteorological Research Institute of Japan 'MRI-AGCM3.2' from the d4PDF project[11] and the Community Atmospheric Model 'CAM5.1.2–0.25degree' from the C20C+D&A project[32]. Both models run 'pre-industrial control' (natural forcings only) and 'historical' (both anthropogenic and natural forcings) simulations, but these models have different experimental settings and integration periods[31–33]. Modelled TC tracks were provided by the individual modelling groups using their own tracking schemes. It is known that different tracking schemes can introduce biases in detected TC frequency changes[25,34,35]. Consequently, we have performed extensive verification of TCs derived from climate model experiments with those obtained using the OWZ scheme but find no notable inconsistencies between results ('Evaluation of detection and tracking schemes' in Methods).

The results from the 20CR dataset show a clear downward trend over the period from 1900 to 2012—as opposed to a weak upward trend in the earlier period—in both global and hemispheric annual numbers of TCs (Fig. 1 and Supplementary Fig. 1). On average, the global annual number of TCs has decreased by ~13% in the twentieth century compared with the pre-industrial baseline 1850–1900 (Fig. 1a). This is consistent with the CAM5 and MRI-AGCM experiments that show a similar TC frequency decline (~11% and ~13%, respectively) when anthropogenic forcing is included (Table 1). Both hemispheres contribute to the global reduction in the annual mean number of TCs (Fig. 1b,c). Importantly, a much larger decline (~23%) is evident after ~1950, coinciding with a period when warming signals in the climate system became evident in the historical record[1,20] (Fig. 1d). We note several change points in the time series of annual TC numbers during the twentieth century (for example, ~1926, 1946 and 1976). Incidentally these change points, which otherwise cannot be resolved in short-term records, coincide with periods of major climate shifts associated with long-term climate variability (such as the Pacific Decadal Oscillation, PDO; additional discussion below). Of interest is the change point around 1946, after which the number of surface observations assimilated into 20CR increased, raising some concerns around the homogeneity of historical proxy records before this period. Thus, to obtain an independent verification of the 20CR-derived decline in global and hemispheric TC numbers, we additionally used the European Centre for Medium-Range Weather Forecasts (ECMWF) Coupled Reanalysis of the Twentieth Century dataset[36] (CERA-20C, Methods). Note that unlike 20CR, CERA-20C is available only from 1901 to 2010, and so we compared changes in the annual mean TC numbers between the two climatological periods: 1901–1950 and 1951–2010, where the latter spans the period of substantial greenhouse warming. As with the 20CR dataset, CERA-20C also supports the decline in both global and hemispheric annual TC numbers for the period under consideration (Table 2).

Annual TC numbers at the basin scale exhibit considerable variability over the period 1850–2012, but statistically significant downward trends are found in every basin since 1850 except the South Indian Ocean where the trend becomes apparent only during the twentieth century (Fig. 2). Several factors can influence both variability and trends so rigorous statistical assessments (Methods) are performed for each basin to ensure that the 'anthropogenic-induced signal' is adequately estimated in the presence of any likely confounding 'background noise' arising from internal climate variability and external forcings such as aerosol changes for the North Atlantic[2,37] (Supplementary Figs. 2 and 3). Such assessments are also necessary to ensure that the presence of any systematic biases in the time series of 20CR TCs are taken into consideration (Supplementary Figs. 4 and 5).

In the Southern Hemisphere, we find statistically significant downward trends for the Australian and South Pacific basins (Fig. 2a,b and Supplementary Fig. 1). Both basins recorded significantly fewer TCs (~11% and ~19%, respectively) during the twentieth century compared with the pre-industrial baseline, and these observed changes are supported by the CAM5 and MRI-AGCM model experiments (Table 1) and by CERA-20C (Table 2 and Supplementary Fig. 4a,b). The South Indian Ocean basin shows little trend from 1850 to 2012 (Fig. 2c), but the trend becomes significantly negative during the twentieth century after accounting for the effects of natural climate variability via Bayesian statistical modelling (Methods on 'Significance test'). Both CAM5 and MRI-AGCM experiments also show a substantial (but statistically insignificant) decline in the annual mean number of TCs between the two climate simulations for the South Indian Ocean basin. It is not clear why the annual mean TC numbers derived from the

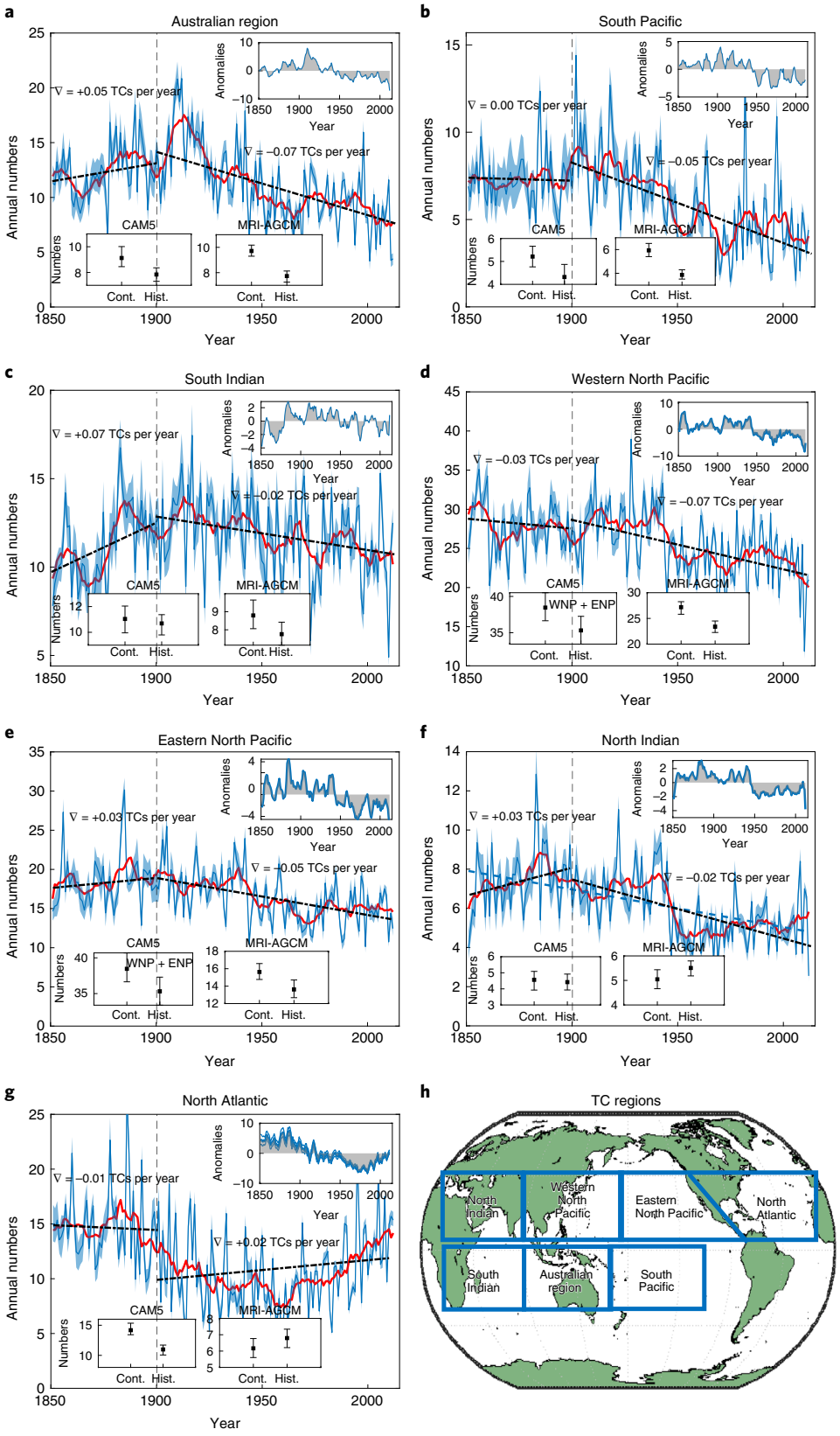

Fig. 2 | Anthropogenic greenhouse warming-induced changes for individual TC basins. a–g, Time series of ensemble-mean TC numbers for the three Southern Hemisphere basins: the Australian region, 90° E–170° E (**a**), the South Pacific, 170° E–120° W (**b**) and South Indian, 0°–90° E (**c**), and four Northern Hemisphere basins: western North Pacific, 100° E–180° E (**d**), eastern North Pacific, 180°–110° W (**e**), North Indian, 0°–90° E (**f**) and North Atlantic, ~110° W–0° (**g**). **h**, The approximate locations of these basins are displayed. Note that due to spatial biases in the western and eastern North Pacific TC genesis locations in the CAM5 simulations, the changes are computed after merging the numbers for these two basins. Insets, colours, shading, confidence intervals and abbreviations are the same as in Fig. 1.

20CR are lower in the pre-industrial period compared with the twentieth century for this basin, even though environmental conditions are more favourable during the earlier period. It seems that decadal variability associated with the PDO, which has a moderately positive association with TC numbers in the basin (Supplementary Fig. 2c), has played a role during the 1850–1900 period when the PDO phase was generally negative.

In the Northern Hemisphere, both the western and eastern North Pacific basins exhibit statistically significant downward trends in the number of TCs since the 1850s (Fig. 2d,e and Supplementary Fig. 1) with ~9% and ~18% fewer TCs forming, respectively, during the twentieth century compared with the pre-industrial baseline. These changes are also consistent with the results from the CAM5 and MRI-AGCM model experiments (Table 1). Note here that TCs simulated in CAM5 have spatial biases in their genesis locations (defined as the first track point in the database) for the neighbouring western and eastern North Pacific basins, and so the change is determined after combining the TC numbers for these two basins. The North Indian Ocean basin also exhibits a statistically significant downward trend, with ~20% fewer TCs recorded during the twentieth century compared with the pre-industrial period, based on 20CR data (Fig. 2f). However, the two climate model experiments indicate no significant change in annual mean TC numbers between the pre-industrial control and the historical simulations. These modelling studies do note that there is poor model performance in representing the influence of increasing Indian subcontinent pollution on Bay of Bengal TCs[38]. We find that the eastern North Pacific and the North Indian Ocean basins have systematic underestimation biases in the time series of annual 20CR TCs compared with the observed records (Supplementary Fig. 5). These biases are consistent through time and so have little influence on the downward trends in both basins. Annual TC numbers derived from CERA-20C for these basins also support the declining trends throughout the twentieth century (Table 2 and Supplementary Fig. 5a–c).

Of particular interest is the North Atlantic basin where there has been an increasing trend in the annual number of TCs over recent decades—probably linked to various internal and external factors including long-term multi-decadal variability[2] and reduced aerosol forcing after the 1970s[37] (Supplementary Fig. 6)—but otherwise no statistically significant trend when an extended period of reconstructed observational data is considered[4,39]. We also note that another study has reported an increasing trend in North Atlantic TC numbers over the past century using a statistical-dynamical downscaling approach[5]. Arguably, these past studies have limitations for climate change trend analysis. For example, downscaling methods—that utilize precursor disturbances (or 'seeds') to evaluate changes in TC characteristics between different climate periods—may not adequately capture the essential physics for generating realistic TC numbers[40]. Such methods assume, either implicitly or explicitly, that adequate seeds are always available, that their rate is independent of climate or that it is controlled by the same environmental factors that control their later development into TCs. Some recent works question these assumptions as they found that seeds can influence TCs independently[14,40]. Other studies that utilize observational records for trend analysis, as discussed earlier, are prone to inhomogeneities arising from changing TC monitoring practices in the basin[41,42]. In contrast, our approach—which circumvents these limitations as discussed earlier—shows a statistically significant downward trend in North Atlantic TC numbers over the entire period 1850–2012 (Fig. 2g). This trend remains statistically robust after accounting for likely aerosol influences and natural climate variability (Supplementary Fig. 3). The overall annual mean number of TCs in the North Atlantic has declined by ~42% during the twentieth century compared with the pre-industrial baseline (~28% after adjusting for an underestimation bias in the time series of 20CR TCs for the post-1970 period, Table 1). This change is consistent

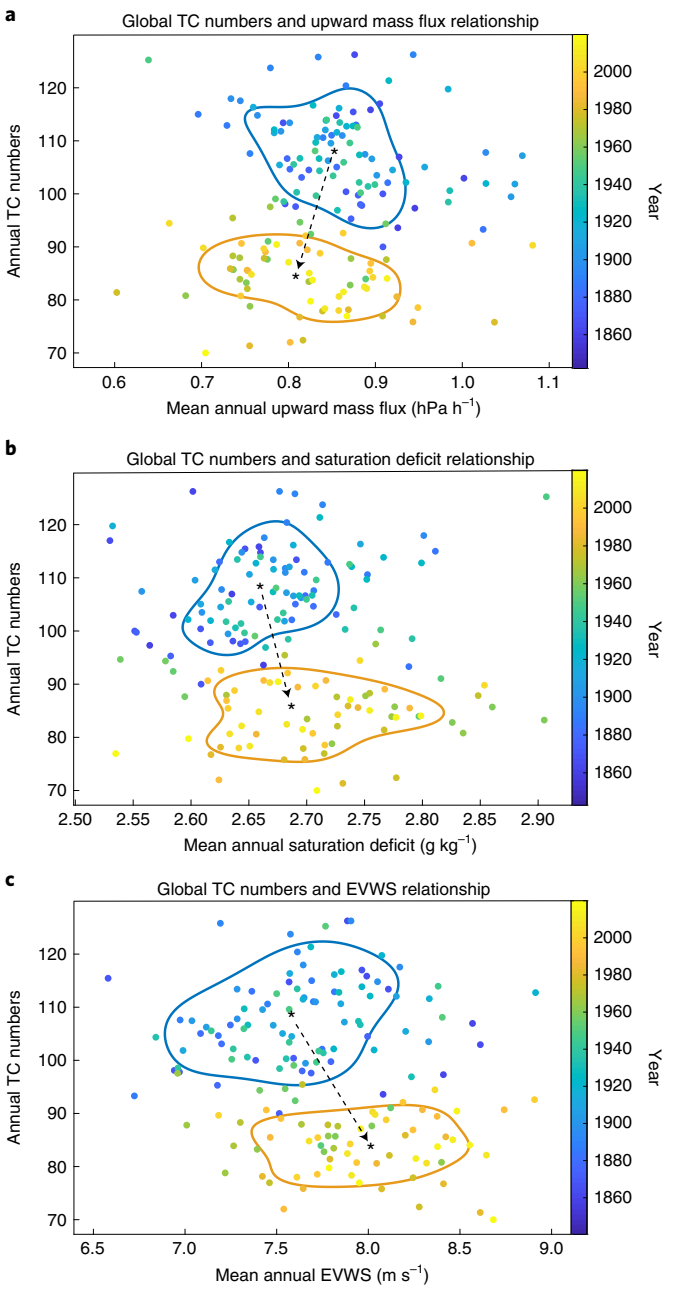

Fig. 3 | Mean annual values of large-scale environmental parameters that are known to influence TC genesis globally. a–c Scatter plots of annual TC numbers mid-tropospheric upward mass flux (**a**), 600 hPa saturation deficit (**b**) and environmental vertical wind shear (EVWS) between the 850 hPa and 200 hPa levels (**c**). Blue and red contours enclose the 50% kernel density estimates of the distribution for the periods 1851–1900 and 1951–2012, respectively. The shift in the centroids (represented by asterisks) associated with the two periods are marked with an arrow. The colour bar denotes corresponding years where the colour scheme is chosen as an indication of the warming over the period as per Fig. 1d.

with the results from the CAM5 experiment that also suggests a statistically significant decline (~22%) in annual mean TC numbers between the pre-industrial control and historical simulations; the MRI-AGCM experiment shows a small (but insignificant) increase in mean TC numbers between the two simulations. When considering only the twentieth century period, both 20CR and CERA-20C show increasing trends in annual TC numbers as with other studies[4],

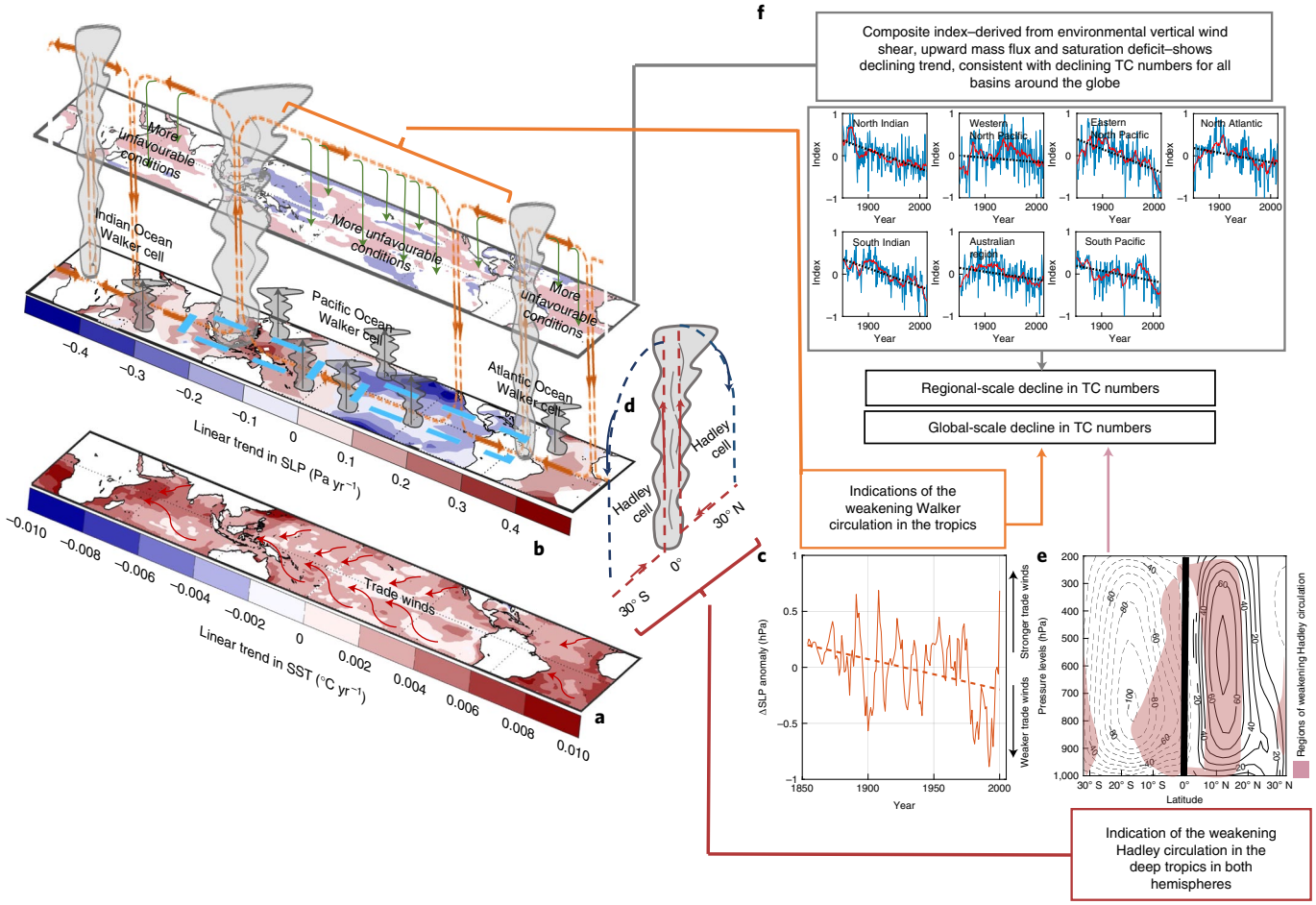

Fig. 4 | Schematic showing the hypothesized link between anthropogenic-induced global warming and associated reduction in annual TC numbers. **a**, Linear trends in SSTs since the mid-nineteenth century, overlaid with the mean trade wind directions (red arrows). **b**, Linear trends in sea-level pressure (SLP) (dashed blue rectangles are used to define the Indo–Pacific SLP gradient, ΔSLP, which serves as a proxy of changes in mean intensity of the Pacific Walker circulation (Supplementary Fig. 10). The three Walker cells are represented in orange. Sinking dry air is represented by green arrows and moist rising air is represented by grey arrows). **c**, Changes in the Indo–Pacific SLP gradient since the mid-nineteenth century. **d**, An illustration of the Hadley circulation. **e**, Observed Hadley circulation pattern, represented by mass stream function of the zonal-mean meridional winds during the period 1900–2012 (red shadings indicate regions where the summertime mean intensity of the circulation has weakened significantly relative to the pre-industrial counterpart (Supplementary Fig. 9)). **f**, Environmental conditions represented as the normalized composite index (Supplementary Figs. 7 and 8).

particularly during the latter half of the century (Table 2 and Supplementary Fig. 5d).

We examine large-scale environmental parameters that are closely related to TC genesis[8–10,13]—environmental vertical wind shear, mid-tropospheric mass flux (indicator of deep convection) and saturation deficit (or mid-tropospheric dryness)—to understand physical causes of the basin-wide downward trends in annual TC numbers over the period 1850–2012. For ease of interpretation, all three large-scale environmental parameters—calculated from 20CR over the main TC development regions for the warmer months of the year, corresponding to the general TC seasons in each hemisphere—are used to derive the normalized composite index for each basin to collectively demonstrate their combined effects on annual TC numbers (Methods). We see declining trends in the normalized composite index over the twentieth century, consistent with the declining trends in TC numbers for each basin (Supplementary Fig. 7). A corollary of these results is that, as the climate has warmed over the twentieth century, decreasing upward mass flux (Fig. 3a), increasing saturation deficit (Fig. 3b) and environmental vertical wind shear (Fig. 3c) have created an environment that is less conducive for TC formation globally (Supplementary Fig. 8). The exact physical mechanisms driving changes in these environmental conditions are still speculative. Here we propose a hypothesis that draws on the link with the observed weakening of the two major atmospheric circulations, the Walker and Hadley circulations[21–24], during the twentieth century compared with the pre-industrial period (Fig. 4 and Supplementary Figs. 9 and 10). Such changes manifest as a reduction of the upward mass flux in the ascending branches of these circulations where substantial tropical deep convection occurs, thus causing a notable reduction in observed TCs globally. At the regional scale, the mid-tropospheric saturation deficit increases as SST increases, leading to greater evaporation and reduced net buoyancy in convective clouds. The reduced mid-tropospheric buoyancy reduces the upward mass flux and increases the potential for dry air entrainment into convective clouds, creating a more hostile environment for TC formation processes.

The 20CR results and the high-resolution climate model results presented here show clear downward trends in global and regional TC numbers between the pre-industrial and the more recent climate period. The downward trend remains robust after accounting for the effects of natural climate variability and aerosol effects for the North Atlantic and basin-specific biases in the 20CR data.

It is hypothesized that these changes are probably due to the twentieth century weakening of the major tropical circulations, which creates more hostile conditions for TC formation. These findings provide new insights that can inform our confidence in future projections of fewer TC numbers associated with greenhouse warming[12]. While the resolutions of the current reanalysis products are too coarse to make conclusions about TC intensity, general consensus from observationally based records suggest an increase in the proportion of severe storms with anthropogenic-induced warming[2]. Going forward, it is anticipated that continued improvement in reanalysis and climate model products and in observational datasets can help identify attributable anthropogenic climate change signals on metrics such as TC intensity and landfalling activities.

Online content

Any methods, additional references, Nature Research reporting summaries, source data, extended data, supplementary information, acknowledgements, peer review information; details of author contributions and competing interests; and statements of data and code availability are available at https://doi.org/10.1038/s41558-022-01388-4.

Received: 15 October 2021; Accepted: 5 May 2022;
Published online: 27 June 2022

References

1. IPCC *Special Report on Global Warming of 1.5 °C* (eds Masson-Delmotte, V. et al) (WMO, 2018).
2. Knutson, T. et al. Tropical cyclones and climate change assessment: part I: detection and attribution. *Bull. Am. Meteorol. Soc.* **100**, 1987–2007 (2019).
3. Lee, T., Knutson, T., Nakaegawa, T., Ying, M. & Cha, E. Third assessment on impacts of climate change on tropical cyclones in the typhoon committee region – Part I: Observed changes, detection and attribution. *Trop. Cyclone Res. Rev.* **9**, 1–22 (2020).
4. Vecchi, G., Landsea, C., Zhang, W., Villarini, G. & Knutson, T. Changes in Atlantic major hurricane frequency since the late-19th century. *Nat. Commun.* **12**, 4054 (2021).
5. Emanuel, K. Atlantic tropical cyclones downscaled from climate reanalyses show increasing activity over past 150 years. *Nat. Commun.* **12**, 7027 (2021).
6. Moon, I., Kim, S. & Chan, J. Climate change and tropical cyclone trend. *Nature* **570**, E3–E5 (2019).
7. Klotzbach, P. & Landsea, C. Extremely intense hurricanes: revisiting Webster et al. (2005) after 10 years. *J. Clim.* **28**, 7621–7629 (2015).
8. Held, I. & Zhao, M. The response of tropical cyclone statistics to an increase in CO_2 with fixed sea surface temperatures. *J. Clim.* **24**, 5353–5364 (2011).
9. Sugi, M. & Yoshimura, J. Decreasing trend of tropical cyclone frequency in 228-year high-resolution AGCM simulations. *Geophys. Res. Lett.* **39**, L19805 (2012).
10. Sugi, M., Murakami, H. & Yoshimura, J. On the mechanism of tropical cyclone frequency changes due to global warming. *J. Meteorol. Soc. Jpn.* **90A**, 397–408 (2012).
11. Yoshida, K., Sugi, M., Mizuta, R., Murakami, H. & Ishii, M. Future changes in tropical cyclone activity in high-resolution large-ensemble simulations. *Geophys. Res. Lett.* **44**, 9910–9917 (2017).
12. Knutson, T. et al. Tropical cyclones and climate change assessment: part II: projected response to anthropogenic warming. *Bull. Am. Meteorol. Soc.* **101**, E303–E322 (2020).
13. Emanuel, K., Sundararajan, R. & Williams, J. Hurricanes and global warming: results from downscaling IPCC AR4 simulations. *Bull. Am. Meteorol. Soc.* **89**, 347–368 (2008).
14. Hsieh, T., Vecchi, G., Yang, W., Held, I. & Garner, S. Large-scale control on the frequency of tropical cyclones and seeds: a consistent relationship across a hierarchy of global atmospheric models. *Clim. Dyn.* **55**, 3177–3196 (2020).
15. Dunkerton, T., Montgomery, M. & Wang, Z. Tropical cyclogenesis in a tropical wave critical layer: easterly waves. *Atmos. Chem. Phys.* **9**, 5587–5646 (2009).
16. Nolan, D. S. What is the trigger for tropical cyclogenesis? *Aust. Meteorol. Mag.* **56**, 241–266 (2007).
17. Gray, W. Global view of the origin of tropical disturbances and storms. *Mon. Weather Rev.* **96**, 669–700 (1968).
18. Ramsay, H. & Sobel, A. Effects of relative and absolute sea surface temperature on tropical cyclone potential intensity using a single-column model. *J. Clim.* **24**, 183–193 (2011).
19. Ting, M., Kossin, J., Camargo, S. & Li, C. Past and future hurricane intensity change along the U.S. East Coast. *Sci. Rep.* **9**, 7795 (2019).
20. Neukom, R., Steiger, N., Gómez-Navarro, J., Wang, J. & Werner, J. No evidence for globally coherent warm and cold periods over the preindustrial Common Era. *Nature* **571**, 550–554 (2019).
21. Vecchi, G. et al. Weakening of tropical Pacific atmospheric circulation due to anthropogenic forcing. *Nature* **441**, 73–76 (2006).
22. Chung, E. et al. Reconciling opposing Walker circulation trends in observations and model projections. *Nat. Clim. Change* **9**, 405–412 (2019).
23. England, M. et al. Recent intensification of wind-driven circulation in the Pacific and the ongoing warming hiatus. *Nat. Clim. Change* **4**, 222–227 (2014).
24. Hu, Y., Huang, H. & Zhou, C. Widening and weakening of the Hadley circulation under global warming. *Sci. Bull.* **63**, 640–644 (2018).
25. Walsh, K. et al. Tropical cyclones and climate change. *WIRES Clim. Change* **7**, 65–89 (2015).
26. Compo, G. et al. The twentieth century reanalysis project. *Q. J. R. Meteorol. Soc.* **137**, 1–28 (2011).
27. Truchelut, R. & Hart, R. Quantifying the possible existence of undocumented Atlantic warm-core cyclones in NOAA/CIRES 20th Century Reanalysis data. *Geophys. Res. Lett.* **38**, L08811 (2011).
28. Truchelut, R., Hart, R. & Luthman, B. Global identification of previously undetected pre-satellite-era tropical cyclone candidates in NOAA/CIRES Twentieth-Century Reanalysis data. *J. Appl. Meteorol. Climatol.* **52**, 2243–2259 (2013).
29. Tory, K., Dare, R., Davidson, N., McBride, J. & Chand, S. The importance of low-deformation vorticity in tropical cyclone formation. *Atmos. Chem. Phys.* **13**, 2115–2132 (2013).
30. Tory, K., Chand, S., Dare, R. & McBride, J. The development and assessment of a model-, grid-, and basin-independent tropical cyclone detection scheme. *J. Clim.* **26**, 5493–5507 (2013).
31. Mizuta, R. et al. Over 5,000 years of ensemble future climate simulations by 60-km global and 20-km regional atmospheric models. *Bull. Am. Meteorol. Soc.* **98**, 1383–1398 (2017).
32. Stone, D. et al. Experiment design of the International CLIVAR C20C+ detection and attribution project. *Weather Clim. Extremes* **24**, 100206 (2019).
33. Wehner, M., Reed, K., Loring, B., Stone, D. & Krishnan, H. Changes in tropical cyclones under stabilized 1.5 and 2.0 °C global warming scenarios as simulated by the Community Atmospheric Model under the HAPPI protocols. *Earth Syst. Dyn.* **9**, 187–195 (2018).
34. Horn, M. et al. Tracking scheme dependence of simulated tropical cyclone response to idealized climate simulations. *J. Clim.* **27**, 9197–9213 (2014).
35. Murakami, H., Hsu, P., Arakawa, O. & Li, T. Influence of model biases on projected future changes in tropical cyclone frequency of occurrence. *J. Clim.* **27**, 2159–2181 (2014).
36. Laloyaux, P. et al. CERA-20C: a coupled reanalysis of the twentieth century. *J. Adv. Model. Earth Syst.* **10**, 1172–1195 (2018).
37. Murakami, H. et al. Detected climatic change in global distribution of tropical cyclones. *Proc. Natl. Acad. Sci. USA* **117**, 10706–10714 (2020).
38. Hazra, A., Mukhopadhyay, P., Taraphdar, S., Chen, J. & Cotton, W. Impact of aerosols on tropical cyclones: an investigation using convection-permitting model simulation. *J. Geophys. Res. Atmos.* **118**, 7157–7168 (2013).
39. Vecchi, G. & Knutson, T. On estimates of historical North Atlantic tropical cyclone activity. *J. Clim.* **21**, 3580–3600 (2008).
40. Sobel, A. et al. Tropical cyclone frequency. *Earth's Future* **9**, e2021EF002275 (2021).
41. Landsea, C., Vecchi, G., Bengtsson, L. & Knutson, T. Impact of duration thresholds on Atlantic tropical cyclone counts. *J. Clim.* **23**, 2508–2519 (2010).
42. Klotzbach, P. et al. Trends in global tropical cyclone activity: 1990–2021. *Geophys. Res. Lett.* **49**, e2021GL095774 (2022).
43. Tory, K., Ye, H. & Brunet, G. Tropical cyclone formation regions in CMIP5 models: a global performance assessment and projected changes. *Clim. Dyn.* **55**, 3213–3237 (2020).

Publisher's note Springer Nature remains neutral with regard to jurisdictional claims in published maps and institutional affiliations.

Open Access This article is licensed under a Creative Commons Attribution 4.0 International License, which permits use, sharing, adaptation, distribution and reproduction in any medium or format, as long as you give appropriate credit to the original author(s) and the source, provide a link to the Creative Commons license, and indicate if changes were made. The images or other third party material in this article are included in the article's Creative Commons license, unless indicated otherwise in a credit line to the material. If material is not included in the article's Creative Commons license and your intended use is not permitted by statutory regulation or exceeds the permitted use, you will need to obtain permission directly from the copyright holder. To view a copy of this license, visit http://creativecommons.org/licenses/by/4.0/.

© The Author(s) 2022

Methods

This section details the data and methods utilized in this study. Particular emphasis is placed on the utility and caveats of data sources and model experiments and on steps being taken to address challenges associated with 'detection and attribution' of TC trends, owing to the lack of global homogeneous TC records.

Definitions. We explore long-term 'detectable anthropogenic changes' in annual TC numbers at global and regional scales. Throughout the paper, the term 'TC trend' is used to refer to a detectable change that is clearly distinguishable from natural variability and is consistent—at least in sign—with climate model experiments attributing changes to anthropogenic influences. 'Natural variability' refers to changes arising from natural processes alone (either forced or from internal variability), without anthropogenic influences[2]. Natural variability dominates the pre-industrial baseline (Fig. 1d), and we use the period 1850–1900—consistent with the IPCC[1]— to define an approximation of the pre-industrial baseline given our TC record extends back to 1850; all changes in annual TC numbers are evaluated relative to this baseline. 'Annual TC numbers' refer to annual counts of TCs that formed in a particular year. For the Southern Hemisphere basins, a TC season extends over two calendar years (that is, from July of the first year to June of the second year). The first year is used to refer to a particular season. For the Northern Hemisphere basins, seasonal TC activity extends over one calendar year (that is, from January to December). The longitudinal bounds of the three Southern Hemisphere and four Northern Hemisphere basins are as follows: the Australian region, 90° E–170° E; South Pacific, 170° E–120° W; South Indian, 0°–90° E; western North Pacific, 100° E–180° E; eastern North Pacific, 180°–110° W; North Indian, 0°–90° E and North Atlantic, ~110° W–0° (Fig. 2h).

Best track data. TC best track data are obtained from multiple sources to serve as a basis of comparison with TC records derived from the 20CR dataset. The International Best Track Archive for Climate Stewardship[44] (IBTrACS)—compiled by the World Meteorological Organization Regional Specialized Meteorological Centers and Tropical Cyclone Warning Centers—provides global coverage of observed TCs, extending farther back to the 1840s, but we utilize data only for the post-satellite period (that is, from 1970) due to data quality issues[45–50]. The Joint Typhoon Warning Center[51] (JTWC) and the US National Hurricane Center database[52] (HURDAT2) provide extended coverage for the western North Pacific (from 1950) and the North Atlantic (from 1878) basins, respectively[53]. The Southwest Pacific Enhanced Archive for Tropical Cyclones[54] (SPEArTC) provides a dataset for the South Pacific basin from 1950.

Reanalysis data. Two reanalysis products are used to derive long-term historical records of TCs globally. These are the Twentieth Century Reanalysis version 2c[26] (20CR) and the ECMWF Coupled Reanalysis of the Twentieth Century[36] (CERA-20C), where the latter is used mainly to verify the 20CR-derived TC trends.

20CR. The 20CR is a state-of-the-art historical reanalysis that assimilates only sea-level pressure (SLP)-based reports, using monthly observed SST and sea-ice distribution as boundary conditions to create a comprehensive record of the atmospheric circulation at sub-daily time scales spanning the period 1850–2012. This surface pressure-based reanalysis is less sensitive to the temporally inhomogeneous observational network, as opposed to modern reanalyses that use available observations at multiple vertical levels and may be prone to larger temporally varying observational biases[55,56]. The 20CR comprises 56 ensemble members with a sufficiently large ensemble spread to provide adequate estimates of uncertainty and confidence in the 20CR-derived TC records. We note that an updated version 3 (20CRv3) has recently become available. This version has been created with improved biases in SLP data before the mid-nineteenth century and with an upgraded data assimilation[55]. The 20CRv3 uses smaller SLP observation perturbations to create the ensemble spread compared with version 2c. While these improvements have resulted in better estimates of measures such as storm intensity[57], the use of a smaller spread is likely to make 20CRv3 more sensitive to 'bogus' IBTrACS entries of TC central pressure in the dataset[55]. Also, we note that some of the fields that are crucial for our TC detector and tracker are not yet available in the 20CRv3, particularly humidity fields at the 700 hPa and 950 hPa levels. Regardless, we subjectively compared several large-scale environmental fields and found no major differences in large-scale fields between the two datasets.

CERA-20C. The CERA-20C is a coupled reanalysis of the twentieth century developed at the ECMWF and has demonstrated substantial ability in representing TCs[36]. Unlike the 20CR data, CERA-20C does not assimilate data from the observed TC database and hence serves as an independent verification of TC trends derived from the 20CR. The CERA-20C dataset is available for the period 1901 to 2010.

Climate model experiments. Data from two projects that involve high-resolution climate model experiments are used here: the 'Database for Policy Decision-Making for Future Climate Change' (d4PDF)[31] and the 'International CLIVAR Climate of the Twentieth Century Plus Detection and Attribution project' (C20C + D&A)[32]. Both of these projects are comprised of 'pre-industrial control' (natural forcings only) and 'historical' (anthropogenic and natural forcings) simulations but with different experimental settings and integration periods (see below).

The d4PDF Project. The d4PD4 project consists of outputs from the Atmospheric General Circulation Model (AGCM) of the Meteorological Research Institute of Japan 'MRI-AGCM3.2', with a 60 km horizontal resolution. Three global warming experimental settings were considered in the d4PD4 project: a historical climate simulation, a +4K future simulation and a non-warming simulation (or control). For the purpose of our study, we utilized data only from the historical and non-warming experiments. The past historical climate consists of a 60-year simulation from 1951 to 2010 with prescribed SST, sea-ice concentration and sea-ice thickness boundary conditions. The duration of the non-warming experiment (referred to as the pre-industrial control) covers the same 60-year period but with the long-term trends removed from the boundary conditions. Altogether, 100 ensemble members were produced for each experimental setting (see ref. [31] for details).

The C20C+D&A project. The C20C + D&A is a subproject within the World Climate Research Programme's International CLIVAR Climate of the Twentieth Century Plus. It is aimed at addressing questions concerning characterization and estimation of historical changes in extreme weather events in the context of anthropogenic-induced global warming (various model output data are available at https://portal.nersc.gov/c20c/data.html). In our case, we utilize the C20C + D&A outputs from the Community Atmospheric Model (CAM5.1.2–0.25degree) for the two experimental settings: the historical 'reference' and the natural historical 'counterfactual' simulations. The 'historical' simulation comprises possible realizations under observed historical climate conditions for the period beginning in 1996 through 2015 (that is, surface and radiative forcings have been varied according to the observational estimates) and well simulates the observed TC counts over this period. The natural historical counterfactual simulations represent the 'world that might have been' without anthropogenic emissions (that is, radiative forcing was set to the pre-industrial 1850 values and the anthropogenic contribution to SST was removed with natural modes of variability preserved). For details on the design and construction of these two experimental settings, see ref. [32] and related documentation. Data are obtained from https://portal.nersc.gov/c20c/experiment.html.

Climate indices and aerosol data. Several climate indices are used to remove the effects of natural climate variability on TC numbers in different basins. We have looked at the effect of aerosols on TC numbers as well. These data are as follows:

- *El Niño Southern Oscillation (ENSO)*. The ENSO Longitude Index (available from https://portal.nersc.gov/cascade/TC/) is used to define the state of ENSO as it tracks the eastward extent of the Walker circulation and therefore reduces the need for Modoki versus canonical ENSO indices[58].
- *Indian Ocean Dipole (IOD)*. The IOD is monitored using the Dipole Mode Index (https://psl.noaa.gov/gcos_wgsp/Timeseries/DMI/).
- *Pacific Decadal Oscillation (PDO)*. The PDO index is obtained from the website https://www.ncdc.noaa.gov/teleconnections/pdo/
- *Atlantic Meridional Overturning Circulation (AMOC)*. Long-term multi-decadal variability can be inferred from the AMOC index, but no direct measurement of the historical AMOC is available before 2004[59]. As the AMOC is known to co-vary with the Atlantic Multidecadal Variability (AMV) mode[60], we therefore use a smoothed version of the AMV index as a proxy of the AMOC. The AMV index is obtained from the website https://psl.noaa.gov/data/timeseries/AMO/.
- *North Atlantic Oscillation (NAO)*. The NAO is a major mode of variability at inter-decadal time scales in the Northern Hemisphere. The NAO indices are obtained from the website https://crudata.uea.ac.uk/cru/data/nao/.
- *Aerosol data*. Historical emissions data (1850–2000) are obtained from: http://tntcat.iiasa.ac.at/RcpDb/dsd?Action=htmlpage&page=download.

TC detection and tracking in reanalyses. We employ an innovative TC detection and tracking scheme called the Okubo–Weiss–Zeta (OWZ) scheme to detect and track TCs in reanalysis datasets (Supplementary Information provides details of its formulation).

TC tracks in model experiments. TC track data from the d4PDF MRI-AGCM3.2 experiments for the historical and non-warming control settings were provided by the Meteorological Research Institute of Japan[11]. Each experimental setting consists of 100 ensemble members for the 60-year period beginning in 1951 and extending through 2010. Similarly, TC track data from the C20C + D&A CAM5 experiments for the historical 'reference' and natural historical 'counterfactual' scenarios were provided by the International CLIVAR C20C + Detection and Attribution project[33].

Evaluation of detection and tracking schemes. It is important to highlight that TC detection and tracking schemes can introduce inconsistencies in TC numbers when applied to reanalysis or model datasets[25,34,35]. There are several different

schemes in existence, each with slightly different formulations and threshold criteria for detecting and tracking TCs. Most of these schemes utilize at least one grid resolution-dependent criteria (such as wind speed and/or lower tropospheric relative vorticity), which leads to much of the disagreement between schemes and models[34].

Obviously, no one detection and tracking scheme is the 'best'. Here we have performed a robust statistical assessment of the 20CR-derived TCs (obtained via the OWZ scheme) with the available observation records and with model-simulated TC numbers from the d4PDF MRI-AGCM3.2 and CAM5 C20C+D&A projects which utilized different schemes. We find substantial agreement between the datasets for all TC basins globally, giving us confidence in TC numbers derived from different schemes (Tables 1 and 2, Supplementary Table 1 and Supplementary Fig. 11). However, an exception is the South Indian basin where, for example, the MRI-AGCM3.2 TCs were slightly underestimated compared with 20CR-derived TCs. TC numbers derived from CAM5 also compare well with those from the MRI-AGCM3.2 experiment globally and for the two hemispheres (Fig. 1 and Table 1). This is also the case for all other basins, except the North Atlantic. Note CAM5 has spatial biases for the eastern and western Pacific, so TC numbers for those basins are combined (for example, Fig. 2). We have also assessed the performance of OWZ and MRI detection and tracking schemes on the 20CR dataset. Results show substantial agreement between the two schemes, giving us further confidence in our methods (Supplementary Fig. 12).

Moreover, it is important to highlight here that some studies have applied downscaling methods to evaluate changes in TC characteristics between different climate periods[5,61]. However, such methods that 'seed' a domain with weak vortices (or disturbances) using a seeding rate that is derived either statistically[5] or from large-scale environmental variables through a genesis potential index[61] may not adequately capture the essential physics for generating realistic TC numbers. These approaches assume, either implicitly or explicitly, that adequate seeds are always available, that their rate is independent of climate or that it is controlled by the same environmental factors as those that control their later development into TCs; these may not necessarily be the case as seeds can influence TCs independently[40].

Statistical assessment of annual TC numbers. It is important to note that all models and reanalyses have limitations and biases in representing spatial and temporal TC distributions. TC detection and tracking schemes are also not free from biases as highlighted earlier. To validate the 20CR-derived TC numbers, comparisons are made with data from observed historical records. Complete TC records are available from the 1970s for all basins when satellite monitoring became available. In the North Atlantic basin, the record is somewhat longer due to aircraft reconnaissance that began in the mid-1940s. This enabled direct comparisons for only a few decades of data for most ocean basins. The independence of the 20CR-derived TCs can also be questioned due to the addition of SLPs from the IBTrACS to represent observed TCs (the 'TC bogus'), which might lead to better performance during the validation period. To address this possible dependence issue, the 20CR TCs are also compared with an alternative reanalysis product (CERA-20C) that does not assimilate any IBTrACS data.

Supplementary Figs. 4 and 5 show annual time series of the 20CR TC numbers compared with observed TCs for the Southern Hemisphere and the Northern Hemisphere basins, respectively. Supplementary Table 1 compares the 'hit rate' and 'false alarm rate' of TCs detected in 20CR with IBTrACS for the period 1989–2012. The hit rate is the ratio of the number of hits divided by the total number of TCs observed, whereas the false alarm rate is the ratio of the number of false alarms divided by the total number of TCs detected. A TC is considered a 'hit' if it occurs in 20CR at the same date/time as the maximum intensity of the observed IBTrACS TC and within a 3.5° latitude radius. We conclude that the 20CR-derived TCs match very well with the observed records for all Southern Hemisphere basins. The hit rate between 20CR TCs and the observed records from the IBTrACS database for the period 1989–2012 are high (that is, above 80% in all cases), with ~86% for the entire Southern Hemisphere (Supplementary Table 1). This shows that, consistent with earlier research[8,9], the 20CR product has substantial skill in realistically reproducing observed TCs for all basins in the Southern Hemisphere.

In the Northern Hemisphere, the 20CR-derived annual TCs for the western North Pacific basin generally agree with the observed records from the IBTrACS database, noting that the TC record quality in IBTrACS is less reliable before the 1940s (Supplementary Data Fig. 5a). The hit rate between the 20CR and IBTrACS TCs for the period 1989–2013 is ~87%. We have also implemented further assessment of our 20CR-derived TC records for the western North Pacific by comparing the meridional oscillation of TCs over Japan and the South China Sea regions with results from two previous studies for the basin[62,63]. After analysing data from 1910 to 2019, Liu et al. showed that for the two periods, 1943–1963 and 1997–2019, the annual number of TCs near Japan are higher than those over the South China Sea, while for the other two periods, 1926–1942 and 1969–1988, the opposite pattern occurs. Together with a similar magnitude of variability, our results also show a similar pattern of the meridional oscillation of TCs near Japan and over the South China Sea (Supplementary Fig. 13). This further indicates the robustness of the 20CR-derived TC records for the western North Pacific basin. However, we note a slight underestimation in the mean 20CR-derived TC numbers for the eastern North Pacific, North Indian and North Atlantic basins (Supplementary Fig. 5b–d). These basins also have hit rates of ~0.54, ~0.80 and ~0.69, respectively (Supplementary Table 1). For the North Atlantic, where the observed TC record extends back to 1851 and has more reliability since 1878 (when the US Signal Service started systematically tracking hurricanes), we find substantially high 15-year running correlation coefficients between the two data sources for the overlapping time period (Supplementary Fig. 5f), giving further confidence in the 20CR-derived TC records. A simple statistical bias correction is implemented to correct the 20CR-derived TCs in the three basins. Because the variance of the two datasets are approximately similar for the overlapping time period (or the reference period over which consistent observational records are available, Supplementary Fig. 5), the 20CR-derived annual TC numbers at time t (T_{RAW}) are simply adjusted by the mean bias ($\overline{O_{REF}} - \overline{T_{REF}}$) present over the reference period to yield bias-corrected 20CR TCs (T_{BC}), such that: $T_{BC}(t) = T_{RAW}(t) + [\overline{O_{REF}} - \overline{T_{REF}}]$. Note that for the North Atlantic, the mean bias correction was applied only for the period 1950–2012 as no bias was present before 1950. We find that the trends remain statistically robust in all Northern Hemisphere basins even after bias corrections are performed, particularly for the North Atlantic where some past studies have shown an increasing trend in the annual number of TCs over recent decades—probably linked to multi-decadal variability[4] and reduced aerosol forcing after the 1970s[2,37], as discussed earlier—but otherwise, no statistically significant trend when an extended period of data is considered (Supplementary Fig. 6) (ref. [39]).

Significance tests. Significance tests for linear trends of annual TC numbers in all basins are implemented using Bayesian statistical models[64–66]. Unlike the frequentist approach, Bayesian models enable us to quantify uncertainties directly by assigning probabilities to model parameters. In the Bayesian framework, all observed and unobserved parameters are given a joint probability distribution, called the prior distribution. The typical Bayesian modelling follows three main steps: capturing available knowledge about a given parameter via the 'prior distribution', which is usually determined before data collection; determining the 'likelihood function' using information about the parameters from the observed data; and combining both the prior distribution and the likelihood function using Bayes' theorem in the form of the 'posterior distribution'. The posterior distribution is then used to make confidence statements about the significance of predictor variables in the model. In our case, predictor variables comprise several modes of natural climate variability that modulate TCs in different basins[67]. An overview of the developing Bayesian model for TC counts is provided in the Supplementary Information (refs. [64–66] provide details of Bayesian statistics and modelling).

The posterior density distribution of model parameters on either side of the zero line provides an indication of the level of contribution of each variable that affects TC numbers in a particular basin. In our case, we have calculated the 95% credible interval (equivalent to the 95% confidence interval using a frequentist statistical approach). If this credible interval lies outside the 'zero' line, then that variable is deemed 'statistically significant'. For example, in the Australian region, a large proportion of the posterior distributions associated with the 'time' variable lie on the left side of the zero line, indicating that the trend is negative and statistically significant at the 95% significance level after accounting for the statistically significant influences from ENSO and the IOD (Supplementary Fig. 2). Similarly, for the North Atlantic, the declining TC trend is statistically significant, with ENSO and the AMOC playing a substantial role in modulating TC variability at interannual and multi-decadal time scales, respectively (Supplementary Fig. 3). Note that we have additionally incorporated here the influence of aerosols on North Atlantic TCs. Aerosols can have a negative impact on TC numbers (as also evident from the posterior distribution plot). Regardless, the downward trend in the North Atlantic basin remains statistically significant even after accounting for the effects of aerosols. All other basins also show statistically significant declining trends in TC numbers, with different modes of natural variability playing varying roles for each basin as also demonstrated in ref. [67]. Also note that the autocorrelation function derived from the model parameter 'time' for each basin reaches zero fairly quickly, indicating no violation of the stationarity assumptions has occurred using our approach.

Environmental parameters. Here we examined three parameters that are closely related to deep convective activity in the tropics and have been widely used to understand changes in TC frequency as a result of anthropogenic warming[8–10,43].

1. *Environmental vertical wind shear*. Defined as the absolute value of the magnitude of the vector difference of zonal and meridional wind components between the 200 hPa and 850 hPa pressure levels such that $\mathrm{EVWS} = \sqrt{(u_{200} - u_{850})^2 + (v_{200} - v_{850})^2}$
2. *Mid-tropospheric mass flux*. Inferred using the 500 hPa ω velocity[10].
3. *Mid-tropospheric saturation deficit*. Difference between the saturation specific humidity q^* and actual specific humidity q at the 600 hPa pressure level[13]. Here q^* is estimated from the saturation vapour pressure e_s such that $q^* = 0.62 e_s(T)/p$ where $e_s = 6.108 e^{\left[\frac{17.27T}{T+237.3}\right]}$ at temperature (T, in °C) and p is the atmospheric pressure (in hPa) (ref. [68]).

These parameters are computed over the tropics when TCs generally form most often during the peak season for each hemisphere (that is, January–March

for the Southern Hemisphere and July–September for the Northern Hemisphere). To demonstrate the combined effects of all three environmental parameters on TC numbers in each basin, we have derived a composite index that constitutes spatially weighted normalized values of the peak season mean environmental vertical wind shear, mid-tropospheric vertical velocity and saturation deficit over the period 1850–2012. Note the index is transformed such that it is directly proportional to changes in TC numbers.

The Walker and Hadley circulations. SST has increased globally at an unprecedented rate since the mid-twentieth century, causing changes in tropical circulations such as in the Walker circulation and the Hadley circulation[21–24]. Since TCs frequently develop within the convective environment of these circulations (that is, regions of convective upward mass flux), it is anticipated that any change in the mean state of the Walker and Hadley circulation will have global impacts on TC activity. The proxies of these two circulations are derived as follows.

- *The Walker circulation*: Indo–Pacific sea-level pressure gradient (ΔSLP) serves as a proxy of zonal winds across the equatorial Pacific and hence is a useful measure of changes in the mean intensity of the Walker circulation. Here ΔSLP is calculated as the difference in monthly values of SLP averaged over the eastern (160° W–80° W, 5° S–5° N) and the western Pacific (80° E–160° E, 5° S–5° N) using data from the Kaplan SLP dataset[69]. Positive (negative) values indicate a strengthened (weakened) Indo–Pacific SLP gradient. The linear trend in ΔSLP provides a long-term change in the strength of the zonal circulation.
- *The Hadley circulation*: The zonal-mean meridional stream function ψ, derived from the meridional wind fields at various pressure levels, serves as a useful measure of the strength and location of the Hadley circulation. Here Ψ is assumed to be non-divergent (that is, conservation of mass transport is satisfied for the global domain). It is computed from the monthly mean data only for the peak TC seasons in each hemisphere (that is, July–September for the Northern Hemisphere and December–February for the Southern Hemisphere) such that:

$$\Psi(p,y) = \frac{2\pi a \mathrm{Cos}(y)}{g}\int_0^P V(p,y)\,dp,$$

where a is the average radius of the earth, g is the gravitational acceleration, V is the zonal-mean meridional wind, p is the pressure level, P is the surface pressure and y is the latitude. The climatological mean vertical structures of stream functions are calculated for the pre-industrial and the twentieth century periods; their difference represents changes in the strength of the Hadley circulation. Statistical significance of the difference is determined (at the 95% level) using the Student's t-test.

We acknowledge that changes in both circulation patterns, particularly over the recent decades, have been at the centre of an intense debate due to inconsistent results between climate models and observations. For example, some studies have attributed the recent strengthening of the Walker circulation to anthropogenic warming[70,71], while others argue that such changes are short term and are largely due to internal climate variability[23,24]. In our case, we utilize a long-term dataset to compute changes between the two climate periods, the pre-industrial and the twentieth century, so the effects of natural variability are negated (for example, Supplementary Figs. 9 and 10).

Data availability

All datasets utilised in this study are publicly available. The 20CR dataset is obtained from https://portal.nersc.gov/archive/home/projects/incite11/www/; d4PDF database is available at http://search.diasjp.net/en/dataset/d4PDF_GCM; C20C+D&A climate model simulations are from the website https://portal.nersc.gov/c20c/data.html; IBTrACS best-track dataset is available at https://www.ncdc.noaa.gov/ibtracs/; JTWC best-track data is obtained from https://www.metoc.navy.mil/jtwc/jtwc.html?best-tracks; the US National Hurricane Center database (HURDAT2) is from https://www.nhc.noaa.gov/data/#hurdat; SPEArTC is from http://apdrc.soest.hawaii.edu/projects/speartc/; climate indices are from https://psl.noaa.gov/data/climateindices/ and the aerosol dataset is available from https://tntcat.iiasa.ac.at/RcpDb/dsd?Action=htmlpage&page=download.

Code availability

The code used for the detection and tracking of tropical cyclones in reanalysis datasets is available at a GitHub repository: https://github.com/savinchand/owz_python with the identifier https://doi.org/10.5281/zenodo.6519260[72].

References

44. Knapp, K., Kruk, M., Levinson, D., Diamond, H. & Neumann, C. The international best track archive for climate stewardship (IBTrACS). *Bull. Am. Meteorol. Soc.* **91**, 363–376 (2010).
45. Holland, G. J. On the quality of the Australian tropical cyclone data base. *Aust. Meteorol. Mag.* **29**, 169–181 (1981).
46. Landsea, C. Climate change: can we detect trends in extreme tropical cyclones? *Science* **313**, 452–454 (2006).
47. Kossin, J., Knapp, K., Vimont, D., Murnane, R. & Harper, B. A globally consistent reanalysis of hurricane variability and trends. *Geophys. Res. Lett.* **34**, L04815 (2007).
48. Chand, S. et al. Review of tropical cyclones in the Australian region: climatology, variability, predictability, and trends. *WIRES Clim. Change* **10**, 1–17 (2019).
49. Harper, B. A., Stroud, S. A., McCormack, M. & West, S. A review of historical tropical cyclone intensity in northwestern Australia and implications for climate change trend analysis. *Aust. Meteorol. Mag.* **57**, 121–141 (2008).
50. Landsea, C. & Franklin, J. Atlantic hurricane database uncertainty and presentation of a new database format. *Mon. Weather Rev.* **141**, 3576–3592 (2013).
51. Chu, J.-H., Sampson, C. R., Levine, A. S. & Fukada, E. The Joint Typhoon Warning Center Tropical Cyclone Best-Tracks, 1945–2000. Naval Research Laboratory Rep. NRL/MR/7540-02-16, 22 pp(2002); https://www.metoc.navy.mil/jtwc/products/best-tracks/tc-bt-report.html
52. Landsea, C. & Franklin, J. Atlantic hurricane database uncertainty and presentation of a new database format. *Mon. Weather Rev.* **141**, 3576–3592 (2013).
53. Schreck, C., Knapp, K. & Kossin, J. The impact of best track discrepancies on global tropical cyclone climatologies using IBTrACS. *Mon. Weather Rev.* **142**, 3881–3899 (2014).
54. Diamond, H., Lorrey, A., Knapp, K. & Levinson, D. Development of an enhanced tropical cyclone tracks database for the southwest Pacific from 1840 to 2010. *Int. J. Climatol.* **32**, 2240–2250 (2011).
55. Slivinski, L. et al. Towards a more reliable historical reanalysis: improvements for version 3 of the Twentieth Century Reanalysis system. *Q. J. R. Meteorol. Soc.* **145**, 2876–2908 (2019).
56. Compo, G., Whitaker, J. & Sardeshmukh, P. Feasibility of a 100-year reanalysis using only surface pressure data. *Bull. Am. Meteorol. Soc.* **87**, 175–190 (2006).
57. Rappin, E., Nolan, D. & Emanuel, K. Thermodynamic control of tropical cyclogenesis in environments of radiative-convective equilibrium with shear. *Q. J. R. Meteorol. Soc.* **136**, 1954–1971 (2010).
58. Williams, I. & Patricola, C. Diversity of ENSO events unified by convective threshold sea surface temperature: a nonlinear ENSO index. *Geophys. Res. Lett.* **45**, 9236–9244 (2018).
59. Yan, X., Zhang, R. & Knutson, T. The role of Atlantic overturning circulation in the recent decline of Atlantic major hurricane frequency. *Nat. Commun.* **8**, 1695 (2017).
60. Sun, C. et al. Atlantic meridional overturning circulation reconstructions and instrumentally observed multidecadal climate variability: a comparison of indicators. *Int. J. Climatol.* **41**, 763–778 (2020).
61. Lee, C., Camargo, S., Sobel, A. & Tippett, M. Statistical–dynamical downscaling projections of tropical cyclone activity in a warming climate: two diverging genesis scenarios. *J. Clim.* **33**, 4815–4834 (2020).
62. Kubota, H. et al. Tropical cyclones over the western north Pacific since the mid-nineteenth century. *Clim. Change* **164**, 29 (2021).
63. Liu, K., Chan, J. & Kubota, H. Meridional oscillation of tropical cyclone activity in the western North Pacific during the past 110 years. *Clim. Change* **164**, 23 (2021).
64. Briggs, W. On the changes in the number and intensity of North Atlantic tropical cyclones. *J. Clim.* **21**, 1387–1402 (2008).
65. van de Schoot, R. et al. Bayesian statistics and modelling. *Nat. Rev. Methods Prim.* **1**, 1–26 (2021).
66. Elsner, J. & Jagger, T. A hierarchical Bayesian approach to seasonal hurricane modeling. *J. Clim.* **17**, 2813–2827 (2004).
67. Chiacchio, M. et al. On the links between meteorological variables, aerosols, and tropical cyclone frequency in individual ocean basins. *J. Geophys. Res. Atmos.* **122**, 802–822 (2017).
68. Murray, F. On the computation of saturation vapor pressure. *J. Appl. Meteorol.* **6**, 203–204 (1967).
69. Kaplan, A., Kushnir, Y. & Cane, M. A. Reduced space optimal interpolation of historical marine sea level pressure. *J. Clim.* **13**, 2987–3002 (2000).
70. Seager, R. et al. Strengthening tropical Pacific zonal sea surface temperature gradient consistent with rising greenhouse gases. *Nat. Clim. Change* **9**, 517–522 (2019).
71. Mitas, C., & Clement, A. Has the Hadley cell been strengthening in recent decades. *Geophys. Res. Lett.* **32**, L03809 (2005).
72. Chand, S. The OWZ tropical cyclone detection and tracking scheme. Zenodo https://doi.org/10.5281/zenodo.6519260 (2022).

Acknowledgements

This work is supported through funding from the Earth Systems and Climate Change Hub of the Australian Government's National Environmental Science Program (NESP). M.F.W. acknowledges support from the Regional and Global Model Analysis (RGMA) programme area of the US Department of Energy's Office of Science under contract number DE-AC02-05CH11231. P.J.K. was funded by the G. Unger Vetlesen Foundation. We also thank G. Compo and L. Slivinski from the US National Oceanic

and Atmospheric Administration Physical Sciences Laboratory for their support around 20CR data access. We thank G. Holland and S. Power for their feedback and U. Khan for information technology-related assistance.

Author contributions

This study was conceived by S.S.C., K.J.E.W., S.J.C., J.K. and J.C.L.C. with inputs from all authors. K.J.T. assisted with the tropical cyclone detection and tracking algorithm. M.F.W. and H.M. provided tropical cyclone track data from the C20C+D&A and d4PD4 projects, respectively. P.J.K. provided long-term historical cyclone tracks for North Atlantic. S.S.C. analysed all data with help from S.S.B., A.J.D. and H.A.R. S.S.C. wrote the manuscript with contributions from all authors.

Competing interests

The authors declare no competing interests.

Additional information

Supplementary information The online version contains supplementary material available at https://doi.org/10.1038/s41558-022-01388-4.

Correspondence and requests for materials should be addressed to Savin S. Chand.

Peer review information *Nature Climate Change* thanks Alexander Baker and the other, anonymous, reviewer(s) for their contribution to the peer review of this work.

Reprints and permissions information is available at www.nature.com/reprints.